Polymer Degradation and Stability 99 (2014) 298–303

Contents lists available at ScienceDirect

Polymer Degradation and Stability

journal homepage: www.elsevier.com/locate/polydegstab

Study on the change of silicon and phosphorus content in the condensed phase during the combustion of epoxy resin with OPS/DOPO

Wenchao Zhang, Xiangmei Li, Rongjie Yang*

National Laboratory of Flame Retardant Materials, School of Materials, Beijing Institute of Technology, 5 South Zhongguancun Street, Haidian District, Beijing 100081, PR China

ARTICLE INFO

Article history:
Received 6 June 2013
Received in revised form
2 October 2013
Accepted 20 October 2013
Available online 29 October 2013

Keywords:
Epoxy resin
Silicon
Phosphorus
Condensed phase
XPS

ABSTRACT

The residues at different time and position of epoxy resin (EP) were obtained during the cone calorimeter tests. The change of Si and P content in these residues during the combustion was obtained by XPS analysis. The result indicates that the Si content reduces at the beginning of fire and the Si element will accumulate with development of fire. These are caused by that, at the beginning of fire, the molten fragment of EP matrix will move upwards and accumulate, but the Si element does not. With development of fire, the product of interaction between the fragment of OPS and decomposition product of EP begins to migrate upwards and accumulate at the surface. However, the P-containing compounds directly migrated upward with the degradation products. The chemical structures of Si-containing and P-containing compounds during the combustion were investigated by the FTIR and XPS. The interactions between DOPO and OPS in the condensed phase happened during the migration process of Si-containing and P-containing compound in the combustion of EP.

1. Introduction

Epoxy resins (EP) have been widely used in surface coating, adhesives, painting, and potting materials, composites, laminates, encapsulants for semiconductor, and insulating materials for electric devices due to their great versatility, toughness, low shrinkage on cure, good moisture resistance, solvent and chemical resistance, outstanding adhesion, and superior electrical and mechanical properties [1–5]. However, as most of the organic polymers, flammability is one of the main drawbacks of the epoxy resins. In order to meet application requirements, their flame retardant properties have been improved while maintenance of other important characteristics such as mechanical and thermal properties and consideration of environmental issues [6–8].

The thermal degradation behaviors of flame retarded epoxy resins with silicon-containing and phosphorus-containing flame-retardants have been reported a lot [9–14]. It can be mainly concluded that the silicon would accumulate on the surface of the char to enhance the thermal stability and char yield, moreover, the phosphorus compounds can promote the char formation and have some additional gas phase flame retardancy [15–19]. The whole paths of silicon and phosphorus migration during the combustion have not been explained in detail. However, in fact, the formation of the char layer is influenced by many factors, such as bubbling, migration, reorientation, agglomeration, ablation, and perhaps also delamination induced thermally and by decomposition [15,20,21]. So it is very difficult to describe the moving path of Si and P element.

In this research, an easy method was used to get the residue at different time and position of epoxy resin (EP) during the combustion. Although we cannot give detailed migration paths of Si-containing and P-containing compounds, we can summarize the Si and P amount in different residue position at different time. Furthermore, the structure of Si-containing and P-containing compounds was reported as well. The change of Si and P amount in the condensed phase is considered to be helpful to understand flame retardant mechanisms of OPS/DOPO.

2. Experimental

2.1. Materials

Diglycidyl ether of biphenol A (DGEBA, E-44, epoxy equivalent = 0.44 mol/100 g) was purchased from FeiCheng DeYuan Chemicals Co., Ltd. The 4,4′-diaminodiphenylsulphone

* Corresponding author.
E-mail address: yrj@bit.edu.cn (R. Yang).

0141-3910/$ – see front matter © 2013 Elsevier Ltd. All rights reserved.
http://dx.doi.org/10.1016/j.polymdegradstab.2013.10.016

(DDS) was purchased from TianJin GuangFu Fine Chemical Research Institute. 9,10-Dihydro-9-oxa-10-phosphaphenanthrene-10-oxide (DOPO) was purchased from Eutec Trading (Shanghai) Co., Ltd. Octaphenyl silsesquioxane (OPS) was synthesized by the hydrolysis and condensation of phenyltrichlorosilane according to a previously reported procedure [22]. The OPS obtained in this way had a perfect T_8 cage structure.

2.2. Preparation of the cured epoxy resins

The cured epoxy resins were obtained using a thermal curing process. At first, DOPO was added to DGEBA by mechanical stirring at 140 °C for 1 h, and then OPS was dispersed in the DGEBA/DOPO for a further 1 h. After that, the curing agent DDS was then added relative to the amount of DGEBA. The equivalent weight ratio of DGEBA to DDS was 9:2. The epoxy resins were cured at 180 °C for 4 h. The contents of OPS and DOPO in the products are listed in Table 1.

2.3. Measurements

Cone calorimeter combustion measurements were performed according to ISO 5660 protocol at an incident radiant flux of 25 kW/m^2 and 50 kW/m^2. The equipment is Fire Testing Technology apparatus with a truncated cone-shaped radiator. The specimen (100 × 100 × 3 mm^3) was measured horizontally without any grids. Typical results from the cone calorimeter tests were reproducible within ±10%, and the reported parameters are the average of three measurements.

To get samples at different time during the combustion, the specimen was cut to four pieces before the cone calorimeter test, and then they are recombined to a whole sample for cone calorimeter test as shown in Fig. 1. The sampling order was from 1 to 4 during the combustion. After a single small sample was taken out from the cone calorimeter test, it will be put out a fire quickly by the cover as shown in Fig. 1. The cap doesn't uncover until the sample is cool. The time of the sampling depended on the normal cone calorimeter test of these samples described above. The samples of char were taken at different position from the residue as shown in Fig. 2. And then the residue was grinded carefully.

All the samples of char was ground carefully and analyzed by FTIR (Nicolet 6700) in ATR mode.

The X-ray photoelectron spectroscopy (XPS) measurements were achieved using a PHI Quantera II system (Ulvac-PHI) at 25 W, 15 kV under a vacuum better than 10^{-6} Pa. The sample was neutralized by both an ion-gun and an electronic-gun. To compensate for sample charging all binding energies were referenced to C1s at 284.9 eV. A variation in the position of each peak of ±0.1 eV was considered to be acceptable.

3. Results and discussion

3.1. Cone calorimeter analysis of EP composites

The heat release rate (HRR) curves of EP/DOPO/OPS under 25 kW/m^2 and 50 kW/m^2 cone calorimeter tests are shown in Fig. 3.

Table 1
Compositions of the investigated EP materials.

Samples	Cured epoxy resin (wt.%)	Content of flame retardant (wt.%)			
		OPS	Si	DOPO	P
Pure EP	100.0	/	/	/	/
EP/DOPO/OPS	89.6	4.1	0.9	6.3	0.9

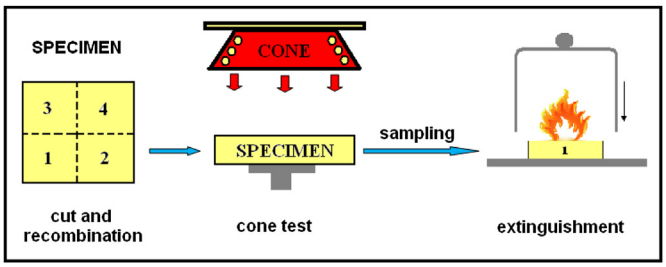

Fig. 1. The sample preparation instruction.

These experiments were used to confirm sampling time. Under 25 kW/m^2 cone calorimeter test, the TTI (time to ignition) of EP/DOPO/OPS was 145 s, but it was 70 s for EP/DOPO/OPS under 50 kW/m^2 cone calorimeter test. As shown in Fig. 3, the peak of heat release rate (p-HRR) of EP/DOPO/OPS under 25 kW/m^2 cone calorimeter test is 341 kW/m^2, but it is 376 kW/m^2 under 50 kW/m^2 cone calorimeter test. Under the different radiant flux, the EP/DOPO/OPS showed different combustion behavior. In order to obtain the variation trend of Si and P amount in the condensed phase during the combustion, the residues obtained from 25 kW/m^2 and 50 kW/m^2 cone calorimeter tests were investigated in detail.

As shown in Fig. 3, the sampling times for 25 kW/m^2 cone calorimeter tests were at 0 s, 150 s, 200 s, 250 s, 300 s, and 350 s. The sampling time for 50 kW/m^2 cone calorimeter tests was at 0 s, 75 s, 125 s, 175 s, 225 s, 275 s, and 325 s.

3.2. Analysis the change of Si and P amount in the condensed phase

The Si and P amount at different time in the condensed phase during 25 kW/m^2 cone calorimeter tests are shown in Fig. 4 and Table 2. The whole XPS data are given in the Supplemental file. There is some inherent error in the determination of the absolute number of counts for an individual element, especially since each sample is different. In Fig. 4, the content of Si and P element was obtained in external, internal, and bottom residues. As shown in Fig. 4A, a quick accumulation of Si element in the bottom residue was detected at 100 s and 200 s. At this time, the content of Si in the external residue is lower than its initial content. The Si amount in bottom residue at 200 s is 6.16% and the Si amount in external residue at 200 s is 0.88% as shown in Table 2. This phenomenon is different from our traditional concept that the Si would accumulate at the surface during the combustion. At the beginning of combustion, the boiling surface can be observed, many molten

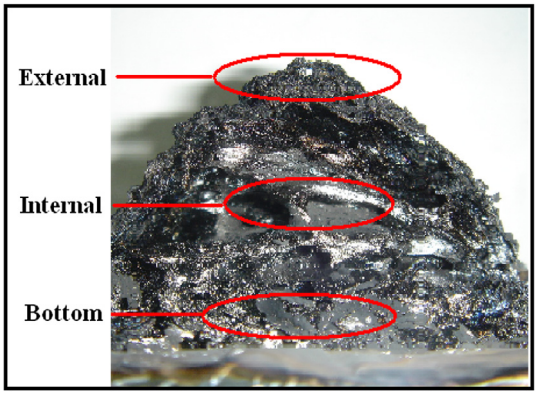

Fig. 2. The positions of different residues.

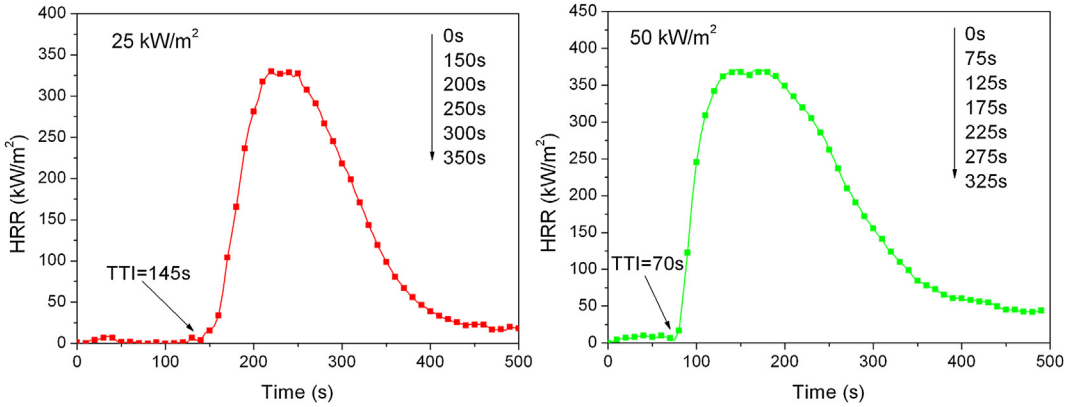

Fig. 3. Heat release rate (HRR) curves of EP/DOPO/OPS under 25 kW/m^2 and 50 kW/m^2 cone calorimeter tests.

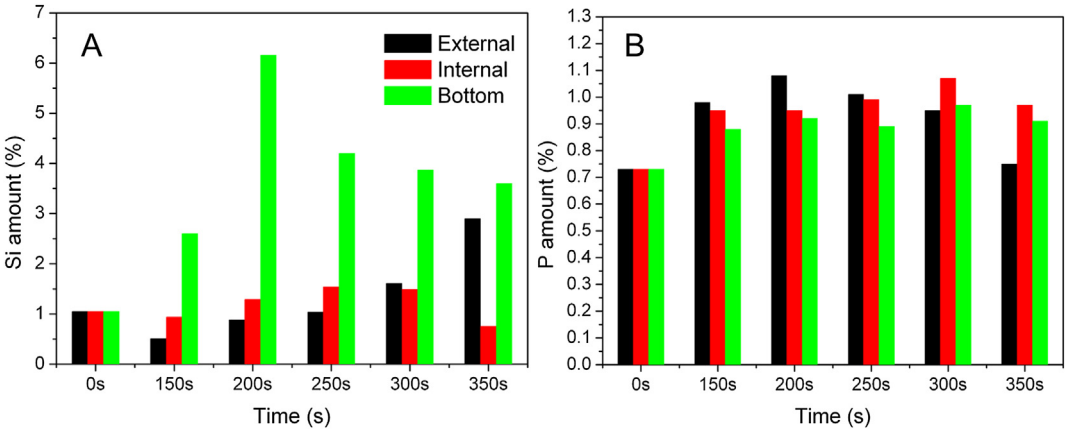

Fig. 4. The Si and P amount at different time in the condensed phase during 25 kW/m^2 cone calorimeter tests.

fragment of EP matrix were taken to the surface with bubbling. This rapidly formed gases and bubbles is expected to be the forces that propel the propagation of the Si element like what happened in the polymer/MMT composites in previous papers [23,24]. However, the OPS has higher thermal stability than the EP matrix [25], thus this force cannot drive the whole OPS molecules to the surface. So with increase of the molten fragment of EP matrix was taken to the surface with bubbling, the Si content in the external char layer reduces, moreover, after upwards moving of EP matrix from the bottom char, the Si content in the bottom residue increases obviously.

In the region of 200 s–350 s in Fig. 4A, the relative content of Si element in external residue increases obviously, but at the same time, the relative contents of Si element in internal and bottom residues reduce gradually. This phenomenon indicates that the Si element begins to migrate and accumulate at the surface of the condensed phase.

In previous papers, many reasons of migration of clay particles to the surface during heating were suggested [26,27], such as temperature gradient, viscosity gradient, gases bubbles, and the interfacial tension. However, there are two main reasons for the accumulation of Si element at surface of the condensed phase. One reason is that flash over consumes lot of other elements (C, O, H). Furthermore, the oxidation after burning during the sampling can also consume some C and H element. Another reason is that the fragment of OPS has reacted with decomposition product of EP, so the Si-containing structure will migrated upwards with bubbling. These two reasons can explain the reason for the increase of Si content in the external char. At the same time, the second reason just can explain the reduction of Si content in the internal and bottom char.

These results indicate that, at the beginning of fire, the molten fragment of EP matrix will move upwards and accumulate, but the Si element does not. With development of fire, the product of interaction between the fragment of OPS and decomposition product of EP begins to migrate upwards and accumulate at the surface. The driving force of these phenomena is the release of gaseous products during the combustion (bubbling) [28,29]. Furthermore, the formations of new structures of Si–O–ph, Si–O–P, and Si–C structure were helpful to the accumulation of Si element in the external residue [14,25].

The content of P in the external, internal, and bottom residue is shown in Fig. 4B, which is quite different from that of Si in Fig. 4A. As shown in Fig. 4B, the change of P amount in the external, internal, and bottom residue can be divided into three stages. They are 0 s–150 s, 150 s–300 s, and 300 s–350 s. Firstly, from 0 s to 150 s, the P amount in the external, internal, and bottom residue increases gradually. Especially for the external residue, the P amount increases from 0.73% to 0.98% as shown in Table 2. And then in the second stage (150 s–300 s), the P amount in the external, internal, and bottom residue keeps steady. In the last stage (300 s–350 s), especially for the external residue, the P amount reduces clearly.

These results the change of P content in the condensed phase is quite different with the change of Si content. This phenomenon is mainly caused by the fact that DOPO can react with DGEBA during

Table 2
XPS data of Si and P amount (%) of EP/DOPO/OPS from 25 kW/m^2 cone calorimeter tests.

Sample	External		Internal		Bottom	
	Si	P	Si	P	Si	P
0 s	1.05 ± 0.33	0.73 ± 0.32	1.05 ± 0.33	0.73 ± 0.32	1.05 ± 0.33	0.73 ± 0.32
150 s	0.51 ± 0.24	0.98 ± 0.22	0.94 ± 0.26	0.95 ± 0.35	2.60 ± 0.75	0.88 ± 0.33
200 s	0.88 ± 0.36	1.08 ± 0.35	1.29 ± 0.28	0.95 ± 0.26	6.16 ± 0.90	0.92 ± 0.29
250 s	1.04 ± 0.22	1.01 ± 0.40	1.54 ± 0.47	0.99 ± 0.34	4.20 ± 0.73	0.89 ± 0.38
300 s	1.61 ± 0.45	0.95 ± 0.34	1.49 ± 0.49	1.07 ± 0.29	3.87 ± 0.38	0.97 ± 0.31
350 s	2.90 ± 0.55	0.75 ± 0.36	0.75 ± 0.35	0.97 ± 0.33	3.60 ± 0.26	0.91 ± 0.45

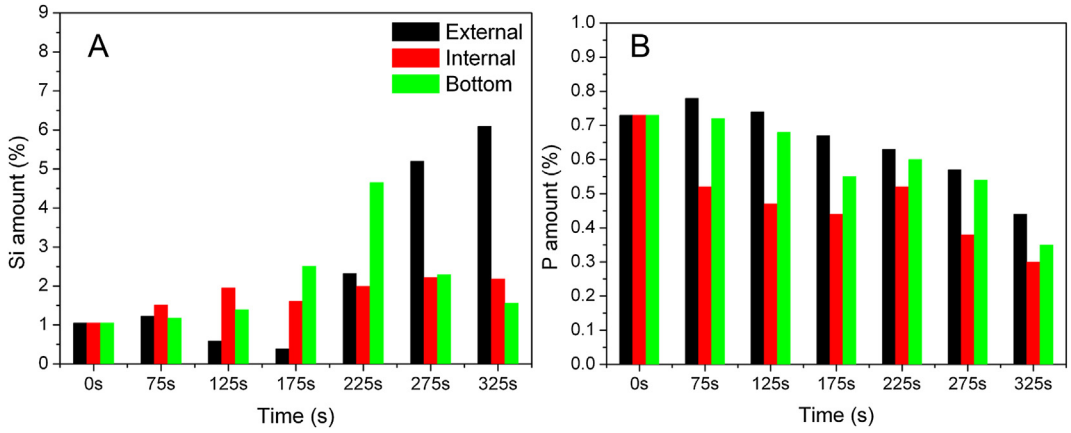

Fig. 5. The Si and P amount at different time in the condensed phase during 50 kW/m^2 cone calorimeter tests.

the preparation process [10,11,14]. This means the DOPO molecule has become part of EP matrix. The P element will migrate with the molten fragment of EP matrix. The enhancement of P amount in the first stage was caused by the reduction of other elements (C, O, H) caused by the initial degradation of EP matrix [30]. The steady P amount during 150 s–300 s means the decompositions of P-containing structures are equal to the decompositions of EP matrix. At last stage, the P-containing structures can decompose quicker than the crosslinking aromatic carbon under the high temperature, which caused the reduction of P amount in the external residue.

To verify the change of Si content during the combustion, the 50 kW/m^2 cone calorimeter tests was achieved to obtain the condensed phase samples. As shown in Fig. 5A, at 175 s, the Si amount in the external residue reduces compared with original Si content, and at the same time, the Si amount in the bottom residue increases obviously. The Si amount in the external residue reduces from 1.05% to 0.39% as shown in Table 3. Then during 175 s–325 s, the Si amount in the external residue increases quickly from 0.39% to 6.09% (Table 3), however, during 225 s–325 s, the Si amount in the bottom residue reduces clearly from 4.65% to 1.56% (Table 3). The whole change of Si amount in the condensed phase in the 50 kW/m^2 cone calorimeter tests is similar to the change of Si content happened in the 25 kW/m^2 cone calorimeter tests.

In Fig. 5B, it is interesting to indicate that the primary trend of P amount in the condensed phase under the 50 kW/m^2 cone calorimeter tests is gradual reduction. This is quite different from the change of P amount in the condensed phase under the 25 kW/m^2 cone calorimeter tests. Nevertheless, this can be the evidence that the P-containing structures decompose quicker than the crosslinking aromatic carbon under the high condensed phase temperature. During 175 s–225 s, a short time increase of P amount in the external and internal residues can be observed. This phenomenon can be caused by the formation of P–O–ph and Si–O–P structures, which process better thermal stability. However, with increase of temperature, these P-containing structures also decomposed quickly and led to the obvious reduction of P amount in 275 s–325 s. Comparing the distributions of P in the external, internal, and bottom residues in Fig. 5B, we can find it is different from Si element done during the combustion process. This result corresponds well with the conclusion about the change P content obtained under 25 kW/m^2 cone calorimeter tests.

Table 3
XPS data of Si and P amount (%) of EP/DOPO/OPS from 50 kW/m^2 cone calorimeter tests.

Sample	External		Internal		Bottom	
	Si	P	Si	P	Si	P
0 s	1.05 ± 0.33	0.73 ± 0.32	1.05 ± 0.33	0.73 ± 0.32	1.05 ± 0.33	0.73 ± 0.32
75 s	1.23 ± 0.25	0.78 ± 0.48	1.51 ± 0.43	0.52 ± 0.21	1.18 ± 0.26	0.72 ± 0.30
125 s	0.59 ± 0.44	0.74 ± 0.44	1.95 ± 0.54	0.47 ± 0.14	1.39 ± 0.25	0.68 ± 0.19
175 s	0.39 ± 0.39	0.67 ± 0.23	1.61 ± 0.24	0.44 ± 0.20	2.51 ± 0.32	0.55 ± 0.26
225 s	2.32 ± 0.67	0.63 ± 0.35	1.99 ± 0.43	0.52 ± 0.25	4.65 ± 0.65	0.60 ± 0.22
275 s	5.20 ± 0.87	0.57 ± 0.45	2.22 ± 0.19	0.38 ± 0.11	2.29 ± 0.17	0.54 ± 0.19
325 s	6.09 ± 0.79	0.44 ± 0.15	2.18 ± 0.34	0.30 ± 0.09	1.56 ± 0.21	0.35 ± 0.20

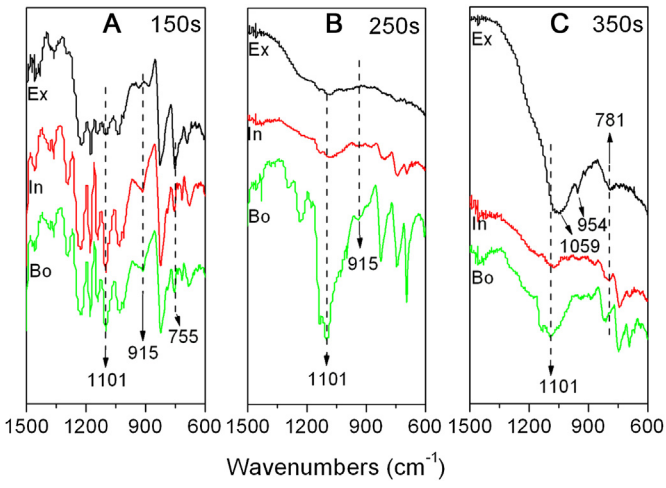

Fig. 6. The FTIR spectra of external (Ex), internal (In), and bottom (Bo) residues at different time during the 25 kW/m^2 cone calorimeter tests.

3.3. Analysis for chemical structures of Si-containing and P-containing compounds during the combustion

3.3.1. FTIR analysis

In order to further understand the reasons for the change of Si and P content during the combustion, the external, internal, and bottom residues obtained at 150 s (just igniting), 250 s, and 350 s combustion during the 25 kW/m^2 cone calorimeter tests were analyzed by the FTIR as shown in Fig. 6. In Fig. 6A, the C–O and Si–O stretching vibrations at 1101 cm^{-1} are detected, moreover, the P–O–phenyl stretching vibration at 915 cm^{-1} and the C–H deformation vibration of phenyl rings of DOPO groups at 755 cm^{-1} are identified also [31,32]. After ignition the absorption at 1101 cm^{-1} in external residue reduces clearly compared with that in internal and bottom residue, which caused by the scission of C–O band in the initial of degradation.

At the same time in Fig. 6A, in the external residue, the P–O–phenyl stretching vibration at 915 cm^{-1} reduces clearly, which means the scission of DOPO. However, the P–O–phenyl stretching vibration of DOPO can be observed in the internal and bottom residues.

In Fig. 6B, an obvious enhancement of absorption at 1101 cm^{-1} can be observed in the bottom residues, which means the big increase of C–O or Si–O structures. The scission of C–O band is the beginning of degradation of EP matrix, so it should not be the increase of C–O structures. According to the XPS analysis above, the Si content in the bottom char increases clearly at this stage. Thus we suspect this result can be caused by the increase of Si–O structures. It should be noticed that the P–O–phenyl stretching vibration at 915 cm^{-1} in internal residue has reduced, but it still remains in the bottom residue.

In Fig. 6C, the most attractive part is the FTIR spectra of external residue which shows several significant changes compared with that of internal residue and bottom residue. The new broad absorbance at 1059 cm^{-1} means new C–O and Si–O structures created in the external residue. A new absorbance peak at 954 cm^{-1} which represents Si–O–phenyl and P–O–phenyl stretching vibrations is detected in the FTIR spectra of external residue [31]. Furthermore, the new absorbance at 781 cm^{-1} represents the C_{Ar}–H deformation vibration further confirms the formation of Si–O–phenyl and P–O–phenyl structures. It should be notice that the absorbance at 1101 cm^{-1} in the bottom residue at 350 s is much lower than that at 250 s, which indicates the upward migration of Si–O structures in this stage. This result corresponds well with the analysis of XPS results.

3.3.2. Si2p and P2p analysis by XPS

The curves of Si2p from the external residues are shown in Fig. 7A. At 150 s, the position of the Si2p peak in the external residue is at 102.8 eV, which means the major Si-containing component process R–Si(–O)$_3$ structures [33]. This kind of component is the fragment of OPS. With the development of the combustion, the slow increase of binding energy of Si2p can be observed. This increase indicates the formation of the Si(–O)$_4$ structures. At 350 s, the position of the Si2p peak in the external residue is at 103.5 eV. This result means the major Si-containing component in 350 s is the Si(–O)$_4$ structures [33].

The curves of P2p from the external residues are shown in Fig. 7B. It has been reported that a binding energy of between 133 and 135 eV can be assigned to P–O–C and PO_3^- groups of phosphates [34]. At 150 s, the position of P2p is at 133.5 eV can be assigned to the –P(=O)–O–C– structure created by the decomposition of DOPO molecules in the residue. With the development of combustion, the peak of P2p increases from 133.5 eV to 134.5 eV. The increase of the P2p binding energies can be explained by the formation of –P(=O)–O–Si– structures. It is reported that the new binding energy of P2p at 134.6 eV is attributed to the formation of –P(=O)–O–Si– linkages in the EP/DOPO/OPS

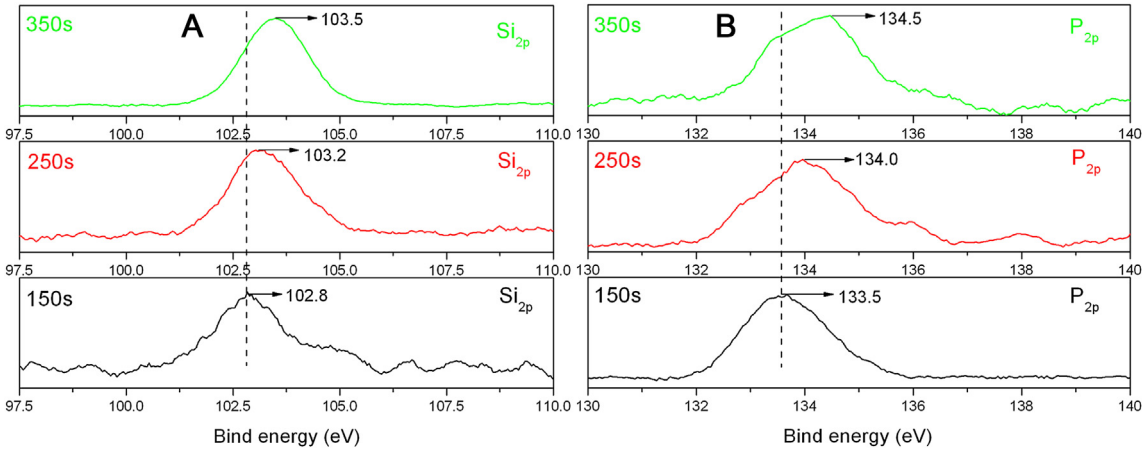

Fig. 7. Si2p and P2p spectra of external residues during 25 kW/m^2 tests.

composites [14]. The formation of –P(=O)–O–Si– during the combustion in the external residue indicates the interactions between DOPO and OPS in the condensed phase exist during the migration of Si-containing and P-containing compound.

4. Conclusions

The Si and P content in the condensed phase of EP/DOPO/OPS composites during the combustion are analyzed by the XPS and FTIR. The XPS results indicate that the Si content reduces at the beginning of fire and the Si element will accumulate with development of fire. These are caused by that, at the beginning of fire, the molten fragment of EP matrix will move upwards and accumulate, but the Si element does not. With development of fire, the product of interaction between the fragment of OPS and decomposition product of EP begins to migrate upwards and accumulate at the surface. In addition, the decomposition of P-containing compound depends on condensed phase temperature a lot, which show that more P-containing compound would remain in the condensed phase at low temperature. The P-containing compound just migrates upwards with the degradation product. The Si2p, and P2p spectra of the residues of EP/DOPO/OPS have been investigated by XPS, which further confirm the migration routes of Si-containing and P-containing compound.

Acknowledgment

This work was funded by National Natural Science Foundation of China (No. 51273023).

Appendix A. Supplementary data

Supplementary data related to this article can be found at http://dx.doi.org/10.1016/j.polymdegradstab.2013.10.016.

References

[1] Schartel B, Balabanovich AI, Braun U, Knoll U, Artner J, Ciesielski M, et al. Pyrolysis of epoxy resins and fire behavior of epoxy resin composites flame-retarded with 9,10-dihydro-9-oxa-10-phosphaphenanthrene-10-oxide additives. J Appl Polym Sci 2007;104:2260–9.
[2] Wang X, Hu Y, Song L, Xing WY, Lu HD, Lv P, et al. Flame retardancy and thermal degradation mechanism of epoxy resin composites based on a DOPO substituted organophosphorus oligomer. Polymer 2010;51:2435–45.
[3] Liu HZ, Zheng SX, Nie KM. Morphology and thermomechanical properties of organic-inorganic hybrid composites involving epoxy resin and an incompletely condensed polyhedral oligomeric silsesquioxane. Macromolecules 2005;38:5088–97.
[4] Brus J, Urbanová M, Strachota A. Epoxy networks reinforced with polyhedral oligomeric silsesquioxane: structure and segmental dynamics as studied by solid-state NMR. Macromolecules 2008;41:372–86.
[5] Liu R, Wang XD. Synthesis, characterization, thermal properties and flame retardancy of a novel nonflammable phosphazene-based epoxy resin. Polym Degrad Stab 2009;94:617–24.
[6] Wang J-S, Liu Y, Zhao H-B, Liu J, Wang D-Y, Song Y-P, et al. Metal compound-enhanced flame retardancy of intumescent epoxy resins containing ammonium polyphosphate. Polym Degrad Stab 2009;94:625–31.
[7] Chow WS, Neoh SS. Dynamic mechanical, thermal, and morphological properties of silane-treated montmorillonite reinforced polycarbonate nanocomposites. J Appl Polym Sci 2009;114:3967–75.
[8] Becker L, Lenoir D, Matuschek G, Kettrup A. Thermal degradation of halogen-free flame retardant epoxides and polycarbonate in air. J Anal Appl Pyrolysis 2001;60:55–67.
[9] Yu D, Kleemeier M, Wu GM, Schartel B, Liu WQ, Hartwig A. Phosphorus and silicon containing low-melting organic-inorganic glasses improve flame retardancy of epoxy/clay composites. Macromol Mater Eng 2011;296:952–64.
[10] Schartel B, Braun U, Balabanovich AI, Artner J, Ciesielski M, Döring M, et al. Pyrolysis and fire behavior of epoxy systems containing a novel 9,10-dihydro-9-oxa-10-phosphaphenanthrene-10-oxide-(DOPO)-based diamino hardener. Eur Polym J 2008;44:704–15.
[11] Perret B, Schartel B, Stoss K, Ciesielski M, Diederichs J, Doring M, et al. Novel DOPO-based flame retardants in high-performance carbon fibre epoxy composites for aviation. Eur Polym J 2011;47:1081–9.
[12] Wang ZF, Liu WQ, Hu CH, Ma SQ. Study on the modification of epoxy resin by a phosphorus- and silica-containing Hybrid. J Appl Polym Sci 2011;121:2213–9.
[13] Spontón M, Mercado LA, Ronda JC, Galià M, Cádiz V. Preparation, thermal properties and flame retardancy of phosphorus- and silicon-containing epoxy resins. Polym Degrad Stab 2008;93:2025–31.
[14] Zhang WC, Li XM, Fan HB, Yang RJ. Study on mechanism of phosphorus–silicon synergistic flame retardancy on epoxy resins. Polym Degrad Stab 2012;97:2241–8.
[15] Schartel B, Weiß A, Sturm H, Kleemeier M, Hartwig A, Vogt C, et al. Layered silicate epoxy nanocomposites: formation of the inorganic-carbonaceous fire protection layer. Polym Adv Technol 2011;22:1581–92.
[16] Sturm H, Schartel B, Weiß A, Braun U. SEM/EDX: advanced investigation of structured fire residues and residue formation. Polym Test 2012;31:606–19.
[17] Karrasch A, Wawrzyn E, Schartel B, Jäger C. Solid-state NMR on thermal and fire residues of bisphenol A polycarbonate/silicone acrylate rubber/bisphenol A bis(diphenyl-phosphate)/(PC/SiR/BDP) and PC/SiR/BDP/zinc borate (PC/SiR/BDP/ZnB)—part I: PC charring and the impact of BDP and ZnB. Polym Degrad Stab 2010;95:2525–33.
[18] Karrasch A, Wawrzyn E, Schartel B, Jäger C. Solid-state NMR on thermal and fire residues of bisphenol A polycarbonate/silicone acrylate rubber/bisphenol A bis(diphenyl-phosphate) (PC/SiR/BDP) and PC/SiR/BDP/zinc borate (PC/SiR/BDP/ZnB)—part II: the influence of SiR. Polym Degrad Stab 2010;95:2534–40.
[19] Wawrzyn E, Schartel B, Seefeldt H, Karrasch A, Jäger C. What reacts with what in bisphenol A polycarbonate/silicon rubber/bisphenol A bis(diphenyl phosphate) during pyrolysis and fire behaviour? Ind Eng Chem Res 2012;51:1244–55.
[20] Lewin M. Some comments on the modes of action of nanocomposites in the flame retardancy of polymers. Fire Mater 2003;27:1–7.
[21] Lewin M, Mey-Marom A, Frank R. Surface free energies of polymeric materials, additives, and minerals. Polym Adv Technol 2005;16:429–41.
[22] Li LM, Li XM, Yang RJ. Mechanical, thermal properties, and flame retardancy of PC/ultrafine octaphenyl-POSS composites. J Appl Polym Sci 2011. http://dx.doi.org/10.1002/app.35443.
[23] Lewin M, Pearce EM, Levon K. Nanocomposites at elevated temperatures: migration and structural changes. Polym Adv Technol 2006;17:226–34.
[24] Lewin M. Reflections on migration of clay and structural changes in nanocomposites. Polym Adv Technol 2006;17:758–63.
[25] Zhang WC, Li XM, Li LM, Yang RJ. Study of the synergistic effect of silicon and phosphorus on the blowing-out effect of epoxy resin composites. Polym Degrad Stab 2012;97:1041–8.
[26] Tang Y, Lewin M. Maleated polypropylene OMMT nanocomposite: annealing, structural changes, exfoliated and migration. Polym Degrad Stab 2007;92:53–60.
[27] Hao J, Lewin M, Wilkie CA. Additional evidence for the migration of clay upon heating of clay-polypropylene nanocomposites from X-ray photoelectron spectroscopy (XPS). Polym Degrad Stab 2006;91:2482–5.
[28] Tang Y, Lewin M. New aspects of migration and flame retardancy in polymer nanocomposites. Polym Degrad Stab 2008;93:1986–95.
[29] Tang Y, Lewin M, Pearce EM. Effects of annealing on the migration behavior of PA6/clay nanocomposites. Macromol Rapid Commun 2006;27:1545–9.
[30] Zhang WC, Li XM, Yang RJ. The degradation and charring of flame retarded Epoxy resin (EP) during the combustion. J Appl Polym Sci 2013. http://dx.doi.org/10.1002/app.39689.
[31] Zhang WC, Li XM, Yang RJ. Pyrolysis and fire behaviour of epoxy resin composites based on a phosphorus-containing polyhedral oligomeric silsesquioxane (DOPO-POSS). Polym Degrad Stab 2011;96:1821–32.
[32] Zhang WC, Li XM, Guo XY, Yang RJ. Mechanical and thermal properties and flame retardancy of phosphorus-containing polyhedral oligomeric silsesquioxane (DOPO-POSS)/polycarbonate composites. Polym Degrad Stab 2010;95:2541–6.
[33] Alexander MR, Short RD, Jones FR, Michaeli W, Blomfield CJ. A study of HMDSO/O_2 plasma deposits using a high-sensitivity and –energy resolution XPS instrument: curve fitting of the Si 2p core level. Appl Surf Sci 1999;137:179–83.
[34] Bourbigot S, Bras ML, Delobel R, Gengembre L. XPS study of an intumescent coating II. Application to the ammonium polyphosphate/pentaerythritol/ethylenic terpolymer fire retardant system with and without synergistic agent. Appl Surf Sci 1997;120:15–29.